Journal of Thermal Analysis and Calorimetry (2024) 149:4209–4225
https://doi.org/10.1007/s10973-024-12940-z

Thermo-hydraulic and entropy generation analysis of nanofluid flow with variable properties in various duct cross sections: a 3-D two-phase approach

Anwesha Varma[1] · **Kottayat Nidhul**[1]

Received: 14 September 2023 / Accepted: 17 January 2024 / Published online: 11 March 2024

Abstract

A three-dimensional computational fluid dynamics (CFD) study is carried out to explore the effect of duct cross section on the thermo-hydraulic performance of various ducts. A finite volume-based scheme with an SST *k*-omega model and mixture model (two-phase model) was used to obtain more realistic results. A two-phase mixture model was used to consider the movement between base fluid and nanoparticles. Al_2O_3 nanoparticle having a volume fraction of 0.01% and 42 nm as particle size, the heat transfer and friction factor characteristic are studied for turbulent flow regime ($3000 < Re < 9000$) with variable thermo-physical properties. A maximum enhancement of 86% in heat transfer rate is obtained for the serpentine duct compared to the conventional circular duct at $Re = 4500$. Owing to a significantly lower increase in pressure drop, the elliptical duct has the highest thermo-hydraulic performance parameter of 1.54 relative to the circular duct. Further, to analyze the heat transfer quality, the entropy generation rate is studied, and it is observed that the square duct reported the highest with an increase of 60% and the elliptical duct the lowest with a reduction of 54% relative to the circular duct. This study can aid in choosing the duct geometry to enhance the heat transfer rate with nanofluid for applications such as solar-thermal, heat exchangers, etc.

Keywords Nanofluid · Turbulent flow · Thermo-hydraulic performance parameter · Mixture model · Entropy generation

Abbreviations

A	Amplitude, m
CFD	Computational Fluid Dynamics
d_p	Diameter of nanoparticle, m
ρ_p	Density of particle, kg m^{-3}
μ_f	Dynamic Viscosity of fluid
T_f	Fluid Temperature, K
f	Friction factor
f_{ref}	Friction factor of circular geometry
q	Heat Flux, W m^{-2}
h	Heat transfer coefficient, W m^{-2} K^{-1}
D_h	Hydraulic Diameter, m
L	Length, m
ΔP	Pressure Drop, Pa
Nu	Nusselt Number
Nu_{ref}	Nusselt Number of reference geometry
k	Thermal Conductivity, W m^{-1} K^{-1}
ε	Thermo-hydraulic Performance Parameter
S_{gen}	Total heat generation
TKE	Turbulence Kinetic Energy, m^2 s^{-2}
Re	Reynolds Number
U	Velocity, m s^{-1}
ϕ_p	Volume Fraction of particle
T_w	Wall Temperature, K
λ	Wavelength, m

Introduction

One of the primary concerns of studies on thermal systems is the amelioration of heat transfer rate with a minimal additional pressure drop that can offset the gains achieved. Compared to fluids, metallic solids have a higher thermal conductivity, making them a feasible alternative for thermal flow devices. The next task is to figure out the size of the particles and the concentration that is to be used. Particle sizes in the range of millimeters or micrometers can cause sedimentation

✉ Kottayat Nidhul
nidhul07@gmail.com; nidhul.k@manipal.edu

[1] Department of Mechanical and Industrial Engineering, Renewable Energy Center, Manipal Institute of Technology, Manipal Academy of Higher Education, Manipal, Karnataka 576104, India

or settling of particles at the bottom of the base fluid due to gravitational effects. Hence, the nanoscale range of size is preferred for these particles, and when they are added to the base fluid, it is called a nanofluid [1]. Additionally, as the surface area is higher than micro-size particles, the thermal response is faster to cause the temperature change when used in a base fluid. In 1993, particles such as oxides of aluminum, titanium, and silicon were used within a size range of 1 and 100 nm in water [1]. The thermal conductivity and viscosity of the fluid increased with the addition of the particles by 32% and 11%, respectively. Later, Choi [2] named the mixture "nanofluid," which can enhance the heat transfer rate in a given size thermal system, thereby saving material expense and size. Nanofluids have been employed for various heat transfer applications, such as industrial cooling applications, smart fluids disseminating heat from battery-operated compact electronic devices, and coolants in nuclear reactors and automobile engines. In recent times, studies have reported the application of ultrasonic vibration in nanofluid heat exchangers and liquid-cooled CPUs resulting in higher outlet temperatures [3].

Enhanced thermal conductivity makes them a feasible choice for enhancing heat transfer rates. With copper as nanoparticles in ethylene glycol, Eastmann et al. [4] reported a 40% increase in thermal conductivity for a concentration of $\varphi = 0.3\%$. Lee et al. [5] obtained a 3% to 23% enhancement for oxides of aluminum and copper nanoparticles in water and ethylene glycol for volume φ in the range of 1 to 4%. For a similar configuration, Das et al. [6] reported a 2 to 36% enhancement for various inlet temperatures. Wen and Ding [7] used γ-Al_2O_3 nanoparticles in de-ionized water for $0.19 < \varphi < 1.6$ and reported a 10% increase in thermal conductivity. Chon et al. [8] developed an empirical correlation with temperature and particle size as variables for determining nanofluid thermal conductivity. Chopkar et al. [9] prepared ethylene glycol and Al70Cu30 nanofluid for a volume fraction less than 1% and observed an increase of 1.2 to 2 times increase in thermal conductivity. For CuO, SiO_2, and multi-walled carbon nanotubes in various base fluids, Hwang et al. [10] reported a 1.05 to 1.09 increase in thermal conductivity for fixed particle size and varying concentration. Li and Peterson [11] studied Al_2O_3 and CuO nanoparticles in water at varying temperatures (27.5 to 33.4 °C) and obtained an increase in thermal conductivity in the range of 1.15 to 1.51. Liu et al. [11] studied Cu-water nanofluid for concentrations less than 0.2% for varying particle diameters from 50 to 300 and reported that smaller particle diameters contribute to maximum thermal conductivity enhancement of 1.24.

When considering the size variation for spherical shape nanoparticles, it is obtained that variation in thermal conductivity for nanoparticles in water and ethylene glycol is not monotonic, and results are non-conclusive. This was due to the uncertainties in the specifications provided in the research articles, as the particle size and shape are often reported from the powder manufacturer's datasheet [12]. Base fluid also influences the thermal conductivity of the resulting nanofluid apart from nanoparticle size, shape, and concentration. Xie et al. [13] studied three base fluids for Al_2O_3 of similar size and concentration and reported that enhancement in thermal conductivity is higher for a base fluid with lower thermal conductivity. Since heat transfer augmentation is required for lower thermal conductivity fluids, the above observation was an encouraging aspect for many applications involving working fluids with low thermal conductivity.

Even though nanofluids result from dispersing nanoparticles in a fluid, for numerical analyses, certain assumptions are made, and nanofluids are modeled as single-phase. The analyses can be done using the homogenous, dispersion and Buongiorno model, wherein governing equations are solved only for the liquid phase. The homogenous model assumes that the particle size is ultrafine; and hence, the slip of nanoparticles and base fluids can be negligible [14]. Further, this model neglects internal forces and thermal exchange between them with an assumption of effective fluid properties. Using a homogenous model, Saha and Paul [15] numerically studied the effect of oxides of aluminum and titanium in water on the heat transfer features of a horizontal tube. They reported that apart from flow velocity, particle concentration and size also influenced the entropy generation and heat transfer rate. Demir et al. [16] studied a similar nanofluid for constant wall temperature for various ϕ using a single-phase homogenous model and reported the trade-off between increased heat transfer and accompanying pressure drop. Later, the heat transfer characteristics of crossflow around the tube bank were studied for constant wall temperature with Al_2O_3 nanofluid for laminar flow and reported that heat transfer rate augmentation can be calculated using the ratio of properties to the fluid [17].

As the random motion of nanoparticles causes energy exchange along with small changes in velocity and temperature in nanofluids, Xuan and Roetzel [18] modified the homogenous model and introduced the thermal dispersion model. Later, Khanafer et al. [19] and Mojarrad et al. [20] developed correlations for determining thermal conductivity in the dispersion model. Using this model, Kumar et al. [21] analyzed Cu-water nanofluid and observed that the dispersion model shows a significant effect of nanoparticles on thermal boundary layer thickness in a two-dimensional cavity. Also, they reported increased thermal conductivity in the zones where velocity was maximum. Later, using the same model, the laminar flow of nanofluid in circular tubes results agreed with the experimental results [22, 23]. Further, the non-uniform distribution of nanoparticles in circular tubes was studied using various nanoparticles in water [23–25]

As the movement between nanoparticles and base fluid molecules has to be considered to obtain more realistic results, two-phase modeling was employed, wherein two different phases were modeled for nanoparticles and fluid [26]. The nanoparticles, under these conditions, move relative to the base fluid with a slip velocity. In the mixture model, each phase is assumed to have different velocity and concentration regions wherein the base fluid influences nanoparticles using drag and turbulence [27]. While the nanoparticles reduce the momentum and turbulence dissipation of the base fluid. Compared to the VOF model, this allows for different phase velocities and requires less computational time for acceptable accuracy in various two-phase problems [28]. Owing to this, most of the studies on nanofluid have used the mixture model. Labib et al. [29] studied the effect of Al_2O_3 in both water and ethylene glycol for laminar flow and reported a higher heat transfer rate with the latter. Then they combined Al_2O_3 and CNTs in water, as hybrid nanofluids and observed that the augmentation in convective heat transfer was significant owing to shear thinning behavior resulting in thinner boundary layer. Similarly, the heat transfer performance of Al_2O_3–Cu hybrid nanofluid was compared to Al_2O_3 nanofluid for laminar flow, and it was reported that the hybrid nanofluid enhanced the heat transfer rate by 4.7% [30]. With Al_2O_3 nanofluid, Mirmasoumi and Behzadmehr [31] reported that nanoparticle concentration in the fully developed regions does not significantly impact the hydraulic parameters. Heat transfer and entropy generation for flow inside an annular pipe with a porous medium were studied for Al_2O_3-water as a working fluid [32]. For increased concentration and porous thickness, thermal entropy generation decreased; while, the frictional part increased. For laminar forced convection using Al_2O_3-water, Moraveji and Ardehali [33] proved that the mixture model was the best compared to the single phase, VOF, and Eulerian model considering the accuracy and speed of computations.

For various duct cross sections in the twisted mini channels, namely square, rectangular, triangular, and elliptical, Khoshvaght-Aliabadi et al. [34] reported that thermo-hydraulic performance was maximum for a nanofluid concentration of 1% in laminar flow regime. With helical tubes, heat transfer rate enhancement was significant owing to centrifugal force and improved heat conduction with a 3% volume fraction [35]. In car radiators made of flat tubes, using alumina nanoparticles with water and ethylene glycol as base fluids resulted in significantly higher heat transfer rates of up to 40% [36]. Ghasemi et al. [37] studied the laminar convective heat transfer of CuO-water in heat sinks with circular and rectangular cross sections and reported higher values for the latter with lower thermal resistance. In radial flow cooling systems, maximum enhancement in heat transfer was reported to be twice that of the base fluid for a higher volume fraction [38]. For higher volume fractions in circular tubes, the thermal and hydraulic performance of γAl_2O_3 with water and ethylene glycol was studied for laminar and turbulent flow regimes. For laminar flow, enhancement in heat transfer rate was found to be 60%. Whereas for turbulent regimes, higher augmentation in heat transfer coefficient was obtained for entry length.

Apart from studies in the laminar flow regime, the thermal and hydraulic features of nanofluid flow in turbulent flow conditions were also explored. Behzadmehr et al. [39] reported that 1% of Cu in water for flow in a circular tube enhances the heat transfer rate by 15%. Further, they observed that particles can absorb velocity fluctuations and reduce the turbulent kinetic energy. Single phase, mixture model, and Eulerian model were used to simulate nanofluids of similar characteristics in horizontal tubes [40]. They observed that the mixture model gave more precise results than the other two. Further, the increase in volume fraction results in a reduction in the rate of thermal enhancement. The thermal and hydraulic features of Al_2O_3-water inside uniformly heated square tubes revealed that at lower Re, the entropy generation due to heat transfer increases. At lower Re, the entropy generation due to friction dominates [41]. The second law analysis of Al_2O_3 in water and ethylene glycol was investigated in a uniformly heated circular pipe for laminar and turbulent flow [42]. For Al_2O_3 in water, the thermal performance improvement was observed up to $Re = 40000$. But for Al_2O_3 in ethylene glycol, the thermal performance improvement was obtained for $Re < 11$. Hejazian et al. [43] studied the nanofluid flow inside a horizontal circular tube exposed to saturated steam. They reported that the mixture model predicts closer to experimental data, and the heat transfer coefficient increases with an increase in particle volume fraction and Re. Yang et al. [44] studied the heat transfer characteristics of nanofluid in a wavy channel and observed that apart from volume fraction, the wavelength and amplitude of the duct also affect the heat transfer rate.

For different radius ratios annuli, Siavashi and Jamali [45] studied the entropy generation features of TiO_2 in water and reported that radius ratio has a significant impact on entropy generation. Yang et al. [46] studied the impact of rib grooves on the performance of nanofluid in a channel at a constant temperature. It is found that smaller rib grooves enhance the heat transfer rate. Heat transfer characteristics of Al_2O_3 and CuO in water were studied for an equilateral triangular duct with vortex generators [47]. Higher heat transfer enhancement was obtained for Al_2O_3 with a maximum performance of 45% relative to water. For volume fraction less than 2%, the single-phase model predicts the heat transfer behavior accurately. Whereas for higher volume fractions, a mixture model is needed to predict results with reasonable accuracy [48]. Khaboshan & Nazif [49] compared the thermo-hydraulic performance of alternating oval and circular ducts for

similar nanofluid and operating conditions. It is observed that the heat transfer coefficient in alternating oval ducts is higher than circular but at the cost of higher pressure drop. Corrugated channels with different wave shapes were investigated for Al_2O_3 nanofluid [50]. It is found that the highest heat transfer rate is obtained for trapezoidal shape. However, thermo-hydraulic performance is higher for sinusoidal configuration owing to lower phase shift in the duct's shape. Similarly, a comparison of straight channels was carried out with semicircle corrugation and trapezoidal corrugation for Al_2O_3 and SiO_2 in water for lower volume fractions [51]. The highest performance was recorded for trapezoidal corrugation and SiO_2 nanofluid at $\phi = 2\%$. With a hybrid nanofluid in a triangular corrugated channel, a maximum heat transfer enhancement of 26% was obtained owing to interrupting boundary layers [52].

From the literature, it is evident that ample studies have been conducted using nanofluid to enhance the heat transfer rate in the laminar flow regime. However, the studies have not considered the trade-off between enhancement in heat transfer rate to the additional pressure drop due to higher viscosity for the base fluids. In addition, only limited studies have explored the nanofluid flow through ducts in the turbulent flow regime using the two-phase model. Further, there is no study available that has compared the thermo-hydraulic and entropy generation features using a two-phase model in the turbulent regime for various duct cross sections. In this regard, the authors have conducted a numerical study of nanofluid flow in varying cross section ducts in the turbulent flow regime using the two-phase mixture model with variable properties. With a validated methodology, heat transfer and fluid flow characteristics of the ducts were studied. Further, thermo-hydraulic performance parameter and entropy generation rate is also analyzed to determine the quality of heat transfer. With the results obtained, the optimum geometry for lower and higher Re can be predicted, aiding future research for potential applications such as parabolic trough solar collectors [53, 54], compound parabolic concentrators [55]and evacuated tube solar water heaters [56]

Methodology

Description of the problem

In the present study, the forced convection of nanofluid is analyzed through different ducts, and the effect of duct cross section on the heat transfer. The duct geometries are circular (reference geometry), square, triangular, serpentine, and elliptical. With water (base fluid) and alumina particles (nanoparticles), the nanofluid has a volume fraction of 0.01%. The average nanoparticle diameter considered for the simulation is 42 nm. The ducts are designed such that the hydraulic diameter is 0.01 m and the length is 1 m, as shown in Fig. 1. Based on the hydraulic diameter of the geometry, the Reynolds number (Re) is defined and is varied from 3000 to 9000. A uniform heat flux of 5000 W m^2 is applied to the smooth duct walls.

Computational domain and meshing

The ducts are modeled using the Design Modeler of ANSYS 2022 R1. The domain is discretized using poly-hexacore elements, as shown in Fig. 2 for the serpentine duct. It was assured that the wall y + is much less (~ 1) for all the ducts to capture the flow physics of the problem near the walls.

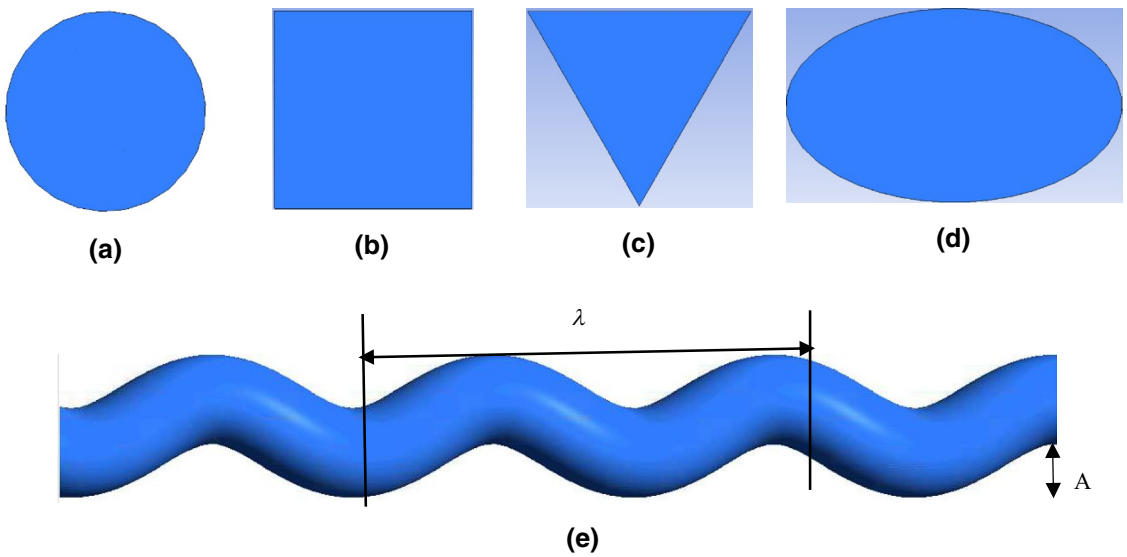

Fig. 1 Various ducts used in this study: **a** circular, **b** square, **c** Triangular, **d** Elliptical, **e** Serpentine

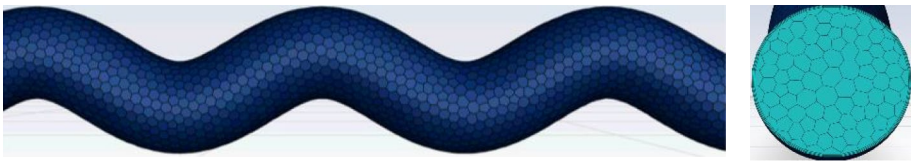

Fig. 2 Serpentine duct domain discretized using poly-hexacore cells

Further, a grid independence study was carried out to ensure that the grid developed is sufficient to produce reasonably accurate results without compromising on the computational time.

CFD analysis

To explore the heat transfer and fluid flow features of nanofluid flow through various duct cross sections, a 3-D CFD simulation is carried out. The governing equations of continuity, momentum, energy, and other boundary conditions are discretized using a Finite volume-based scheme. The pressure–velocity coupling is carried out using Semi Implicit Method for Pressure Linked equations (SIMPLE). With the SST k-omega model, the convergence criteria were set to 1e-6, and the wall temperature was monitored to ensure a steady state.

To obtain more realistic results, the movement between nanoparticles and base fluid molecules was modeled using a two-phase approach. The nanoparticles, under these conditions, move relative to the base fluid with a slip velocity. Using the mixture model, each phase is assumed to have different velocity and concentration regions wherein the base fluid influences nanoparticles using drag and turbulence. It considers the base fluid (water) and nanoparticle (Al_2O_3) to be strongly coupled, and the secondary phase (nanoparticles) closely follows the field. Both phases have their velocity vector fields using the concept of slip velocity and volume concentration inside the considered control volume. Additionally, the primary phase (nanofluid) affects secondary phase flow by exerting drag force [57] on the nanoparticles. It is assumed that the nanoparticles have uniform spherical shape and size.

The volume fraction equation is given as:

$$\nabla \cdot \left(\phi_p \rho_p \overrightarrow{V_m}\right) = \nabla \cdot \left(\phi_p \rho_p \overrightarrow{V_{dr,p}}\right) \tag{1}$$

where $\overrightarrow{V}_m$ is the mixture velocity and is given as

$$\overrightarrow{V_m} = \sum_{s=1}^{n} \frac{\phi_s \rho_s \overrightarrow{V_s}}{\rho_m} \tag{2}$$

where ϕ_s denotes the volume fraction of the phases. Since the phases are water and Al_2O_3, the volume fraction of the nanoparticle and the latter are ϕ_p and (1-ϕ_p), respectively.

Drift velocity or relative velocity corresponding to nanoparticles and the base fluid is determined as follows [58]:

$$\overrightarrow{V_{dr,p}} = \overrightarrow{V_p} - \overrightarrow{V_m} \tag{3}$$

The relation between drift velocity and slip velocity is determined as follows:

$$\overrightarrow{V_{dr,p}} = \overrightarrow{V_{pf}} - \sum_{s=1}^{n} \overrightarrow{V_{pf}} \frac{\phi_p \rho_p}{\rho_m} \tag{4}$$

where $\overrightarrow{V}_{pf}$ is the slip velocity

$$\overrightarrow{V_{pf}} = \frac{\rho_p d_p^2}{18 \mu_f f_{drag}} \frac{\rho_p - \rho_m}{\rho_p} \vec{a} \tag{5}$$

In which acceleration ($\vec{a}$) is given as:

$$a = g - \left(V_m \cdot \nabla\right) V_m \tag{6}$$

Further in this study, nanofluid properties depend upon temperature, incorporated in the simulation using a user-defined function.

To assess the thermo-hydraulic features of various duct configurations studied, the following parameters are employed.

The average heat transfer coefficient over the duct walls are obtained as,

$$h = \frac{q}{T_w - T_f} \tag{7}$$

The average Nusselt number (Nu) is obtained based on the hydraulic diameter of the duct (D_h) and is given by.

$$Nu = \frac{hD_h}{k} \tag{8}$$

Hydraulic performance is evaluated using the friction factor (*f*), given by

$$f = \frac{\Delta P D_h}{2\rho L U^2} \tag{9}$$

Thermo-hydraulic performance parameter (THPP) is evaluated considering the base case as the conventionally used circular duct and is obtained by [59]

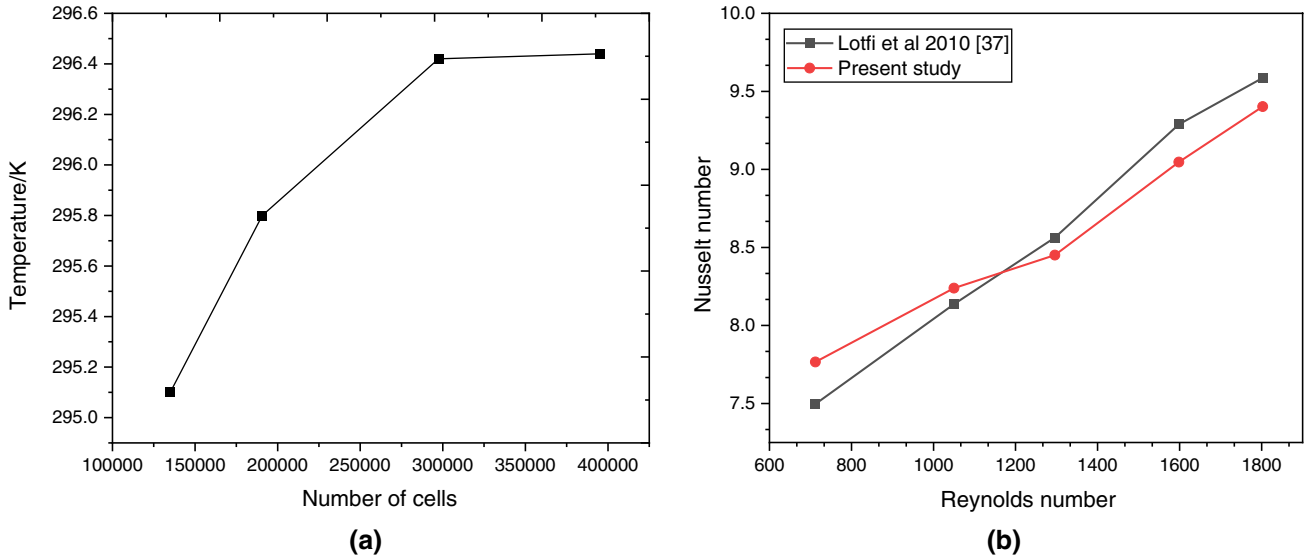

Fig. 3 **a** Grid independence study and **b** comparison of the results of the present CFD study with the experimental results [40]

$$\varepsilon = \frac{\frac{\mathrm{Nu}}{\mathrm{Nu}_{\mathrm{ref}}}}{\left(\frac{f}{f_{\mathrm{ref}}}\right)^{1/3}} \tag{10}$$

To assess the quality of heat transfer, a second law analysis is done using entropy generation analysis, and the expression [60] for the same is given by

$$\begin{aligned} S_{\mathrm{gen}} &= S'''_{\mathrm{HT}} + S'''_{\mathrm{FF}} = \frac{k_{\mathrm{eff}}}{T^2}(\nabla T)^2 + \frac{\mu_{\mathrm{eff}}}{T} \\ \phi &= \frac{k_{nf}}{T^2}\left[\left(\frac{\partial T}{\partial x}\right)^2 + \left(\frac{\partial T}{\partial y}\right)^2 + \left(\frac{\partial T}{\partial z}\right)^2\right] \\ &+ \frac{\mu_{nf}}{T}\left[2\left\{\left(\frac{\partial u}{\partial x}\right)^2 + \left(\frac{\partial v}{\partial y}\right)^2 + \left(\frac{\partial w}{\partial y}\right)^2\right\}\right. \\ &\left. + \left(\frac{\partial u}{\partial y} + \frac{\partial v}{\partial x}\right)^2 + \left(\frac{\partial v}{\partial z} + \frac{\partial w}{\partial x}\right)^2 + \left(\frac{\partial w}{\partial y} + \frac{\partial u}{\partial z}\right)^2\right] \end{aligned} \tag{11}$$

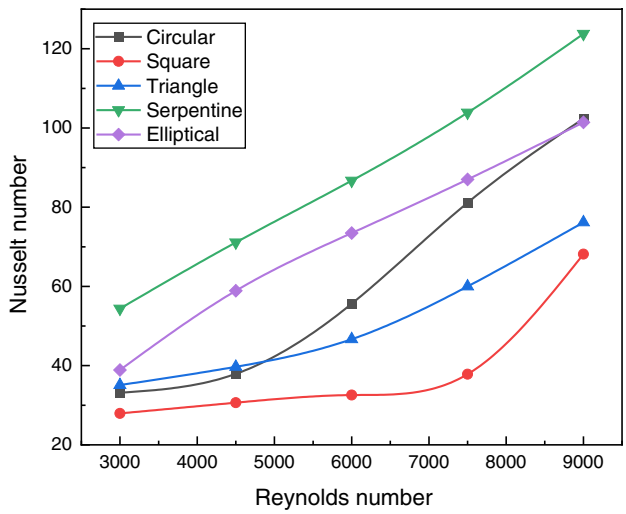

Fig. 4 Variation of Nusselt Number with Reynolds number for different geometries

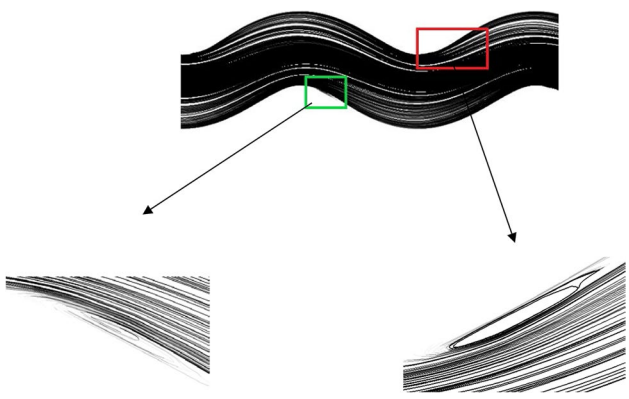

Fig. 5 Streamlines of velocity at the longitudinal plane for serpentine geometry at Re = 9000 with magnified view of recirculation regions at the crest and trough

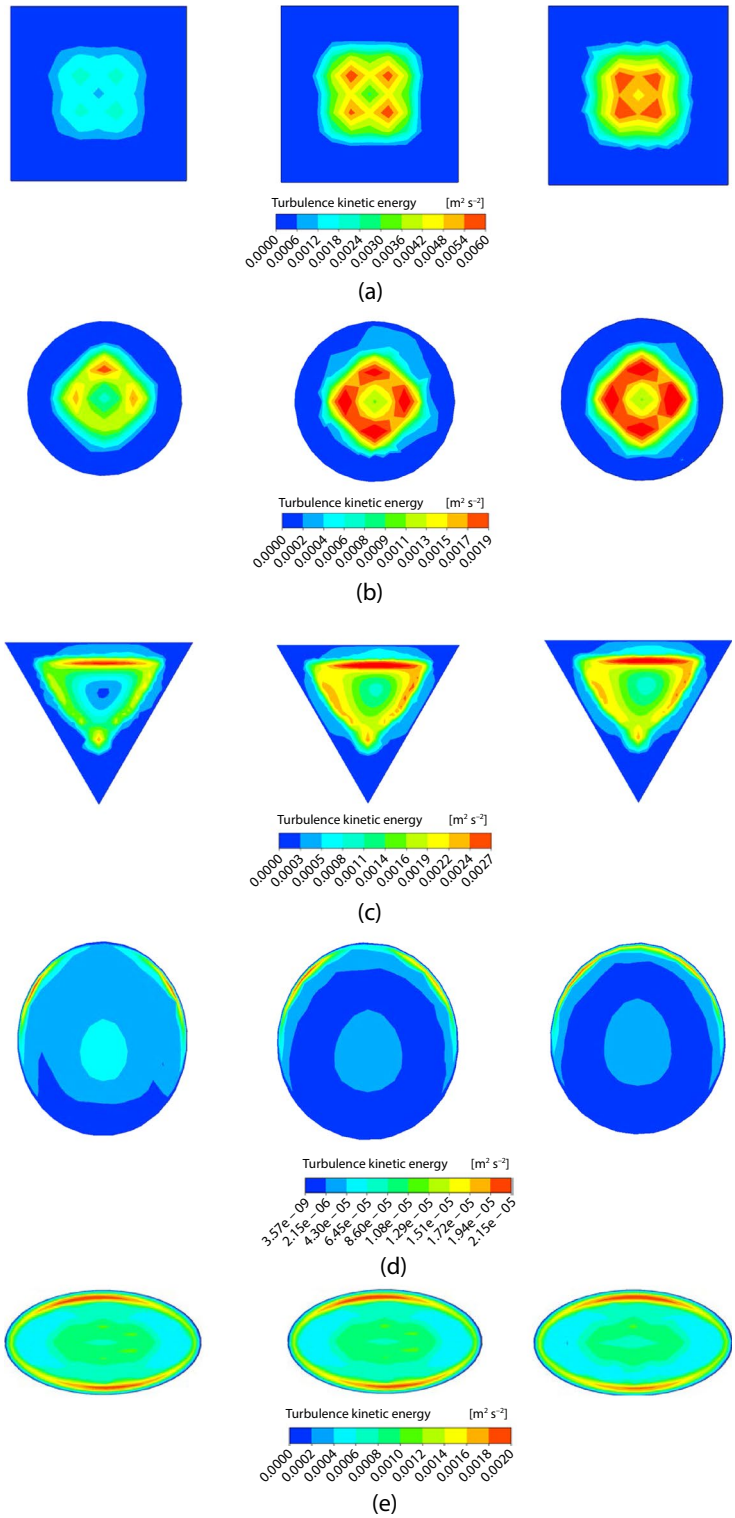

Fig. 6 Turbulent kinetic energy contours for **a** Square, **b** Circular, **c**Triangular, **d** Serpentine and **e** Elliptical at Re = 4500 at various cross-planes

Grid independence and validation

A Grid independence study has been conducted, as shown in Fig. 3a to ensure that there is no discrepancy in the results with grid variation. With the optimum grid size, further simulations are carried out. The results obtained with the present CFD methodology are compared with experimental findings [40], to examine the precision and to ensure reasonable accuracy of the two-phase mixture model for the chosen problem definition (Fig. 3). Upon comparing the Nusselt

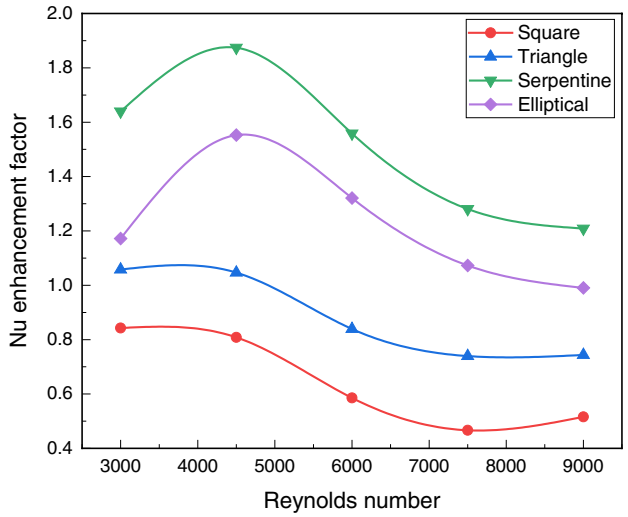

Fig. 7 Variation of Nusselt Enhancement factor with Reynolds for different geometries

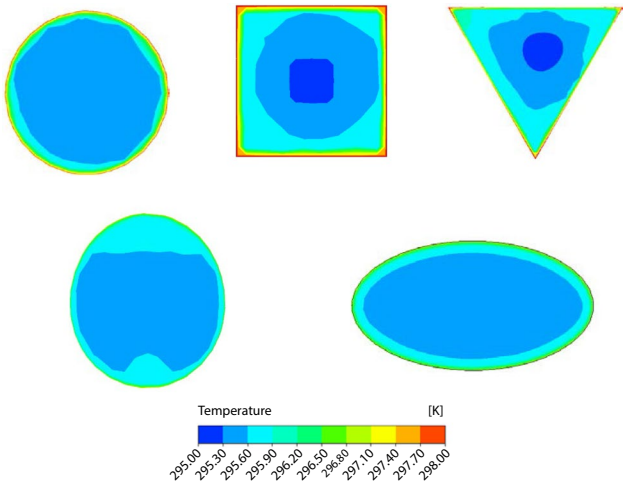

Fig. 9 Fluid temperature contours at the midplane of the various duct geometries for Re = 4500

number (*Nu*) variation with the Reynolds number (Re), it is obtained that the maximum deviation of the present CFD results is 3.4% with an average of 2%. As the results obtained were reasonably accurate, the same methodology has been used to carry out further simulations.

Results and discussion

A 3-D numerical investigation of flow and heat transfer characteristics has been carried out for ducts of various cross sections in the turbulent flow regime ($3000 < Re < 9000$).

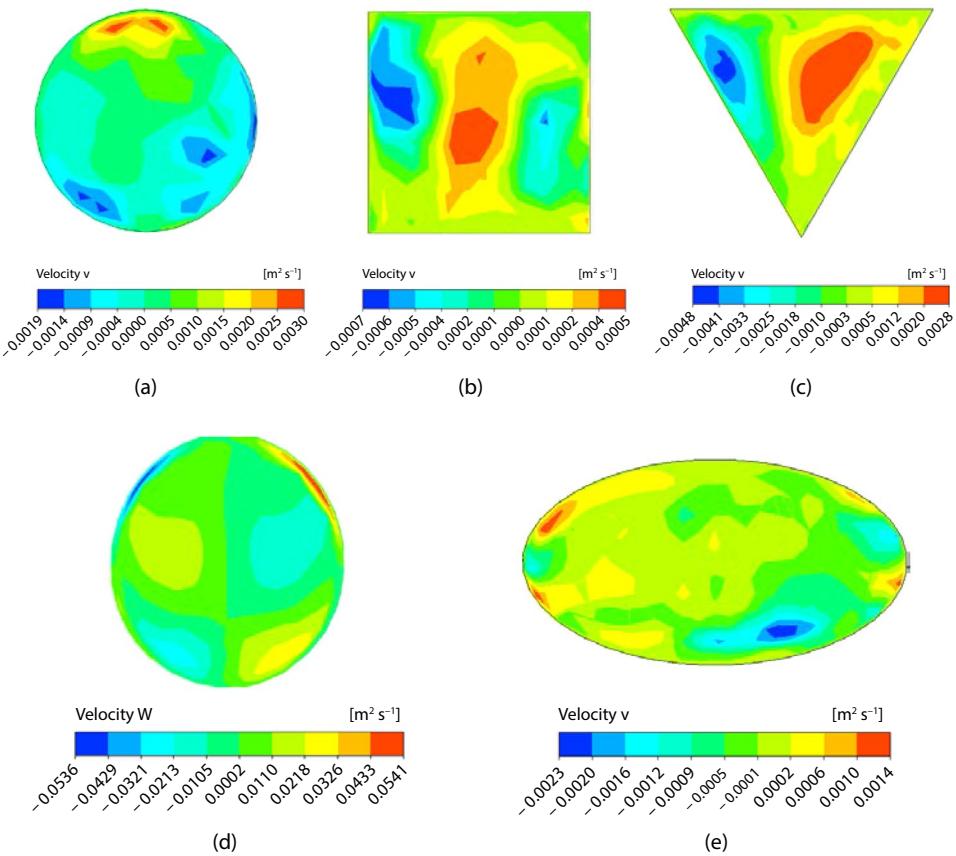

Fig. 8 Secondary flow velocity contours at midplane of the **a** circular, **b** square, **c** triangular, **d** serpentine, **e** elliptical geometry for Re = 4500

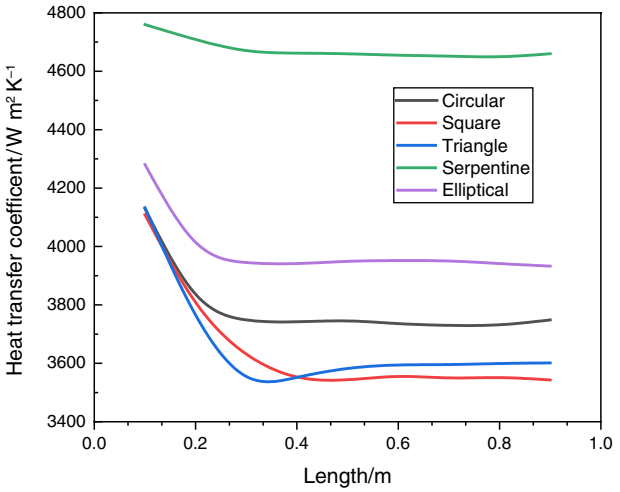

Fig.10 Variation of heat transfer coefficient along the length of the duct for various cross sections for Re = 4500

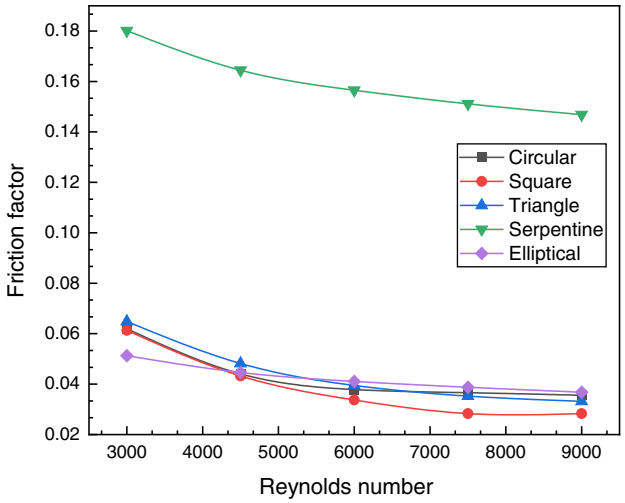

Fig. 11 Variation of Friction factor with Reynolds number for different duct geometries

The cross sectional ducts compared are circular, square, triangular, Serpentine, and elliptical, for a similar hydraulic diameter and length. The findings have been established using characteristic plots such as Nusselt number (*Nu*), friction factor (*f*), Nusselt number enhancement factor, friction factor enhancement, entropy generation (S_{gen}) and thermo-hydraulic performance parameter (*THPP*). Further, for flow visualization, contour plots such as velocity, pressure, turbulent kinetic energy (*TKE*), entropy generation, and streamlines are used.

Heat transfer characteristics

With an increase in Re, it is observed that *Nu* increases for all duct cross sections, attributed to the reduction in boundary layer thickness with an increase in flow velocity (Fig. 4). Upon comparison, it is evident that serpentine duct has the highest heat transfer characteristics for the range of Re. Compared to circular duct, maximum enhancement in *Nu* is 64% at Re = 3000 for serpentine duct. However, for higher Re, the enhancement in *Nu* reduces to 21% owing to recirculation zones formed near the crest and trough, as shown in Fig. 5. The duct with a square cross section has the lowest heat transfer features compared to all other ducts. Upon comparison to the circular, a 54% reduction in *Nu* is obtained. Further, the contours of turbulent kinetic energy (*TKE*) reveal that serpentine and elliptical ducts have higher TKE indicating better mixing and enhanced heat transfer, as shown in Fig. 6.

To evaluate the enhancement in heat transfer rate, the conventional circular geometry is considered as the base geometry. It is observed that Nu enhancement increases with Re up to 4500, and with a further increase, it reduces (Fig. 7). For serpentine and elliptical duct, the enhancement in *Nu* is higher than 1. Whereas, for the triangular duct, beyond Re = 4500, the enhancement in *Nu* drops, and for the square duct, it underperforms the circular duct at all Re. The highest enhancement factor is achieved for serpentine at Re = 4500, having a value of 1.87, and this value decreases subsequently as Re decreases, and a similar trend is exhibited by the elliptical duct.

It is observed that secondary flow near the walls is higher for serpentine and elliptical ducts in comparison with circular and square ducts, wherein it is almost stagnant (Fig. 8). Owing to this, there is a better mixing of hot and cold fluid leading to higher convective heat transfer. It is also worth noting that in the triangular and circular duct, even though the maximum velocity of secondary flow is higher, it is limited to a small portion of the duct walls. This is also evident from the fluid temperature contours Fig. 9, in circular, square, and triangular, the fluid temperatures near the walls are higher, indicating higher viscous resistance. This high-temperature region near the wall acts as thermal resistance reducing the rate of heat transfer.

Further, from the heat transfer variation along the length of the duct (Fig. 10), it is observed that the serpentine duct has a higher heat transfer coefficient for the entire length of the duct. It is observed that due to the presence of crest and trough, the heat transfer coefficient varies along the length with maximum at the crest and minimum at the trough. This is attributed to the separation and re-attachment of the boundary layer. Upon comparison to circular ducts, elliptical and serpentine ducts have higher heat transfer coefficients along the length of the duct; whereas, square and triangular ducts underperform even though the hydrodynamic entry length is higher in both cases. In square duct, the magnitude of heat transfer coefficient along the length of the duct is

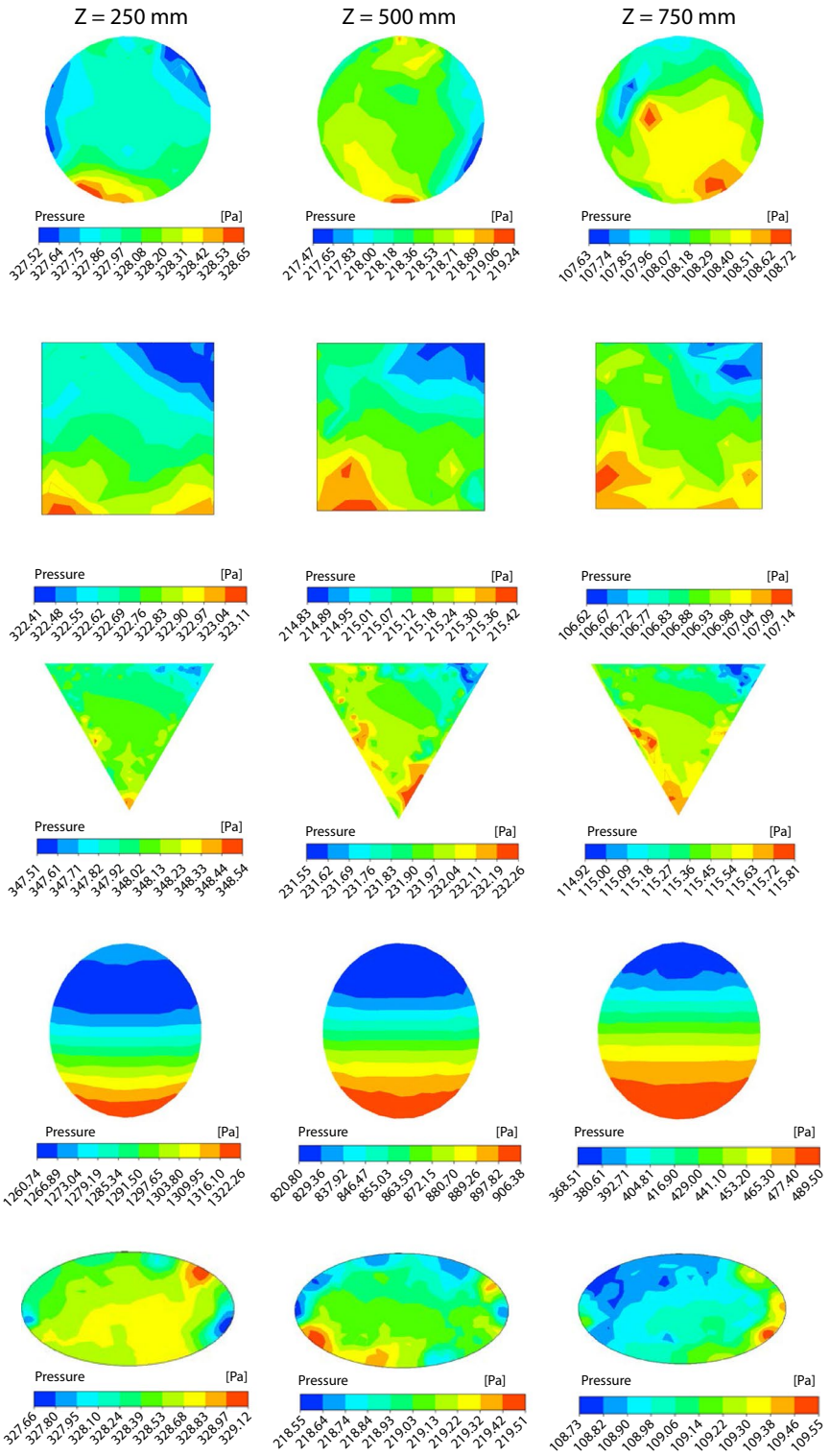

Fig. 12 Static pressure distribution across various cross section planes along the duct length **a** Circular duct, **b** Square duct, **c** Triangular duct, **d** Serpentine duct, **e** Elliptical duct

less than that of circular duct (Fig. 10). Further from Fig. 9, it is observed that temperature of the fluid near the walls is higher for square duct, indicating thicker boundary layer. This high-temperature region acts as a hot spot retarding further heat transfer rate.

Hydraulic characteristics

Whenever heat transfer enhancement occurs, the obvious question is how much the pressure drops or does the increase in pressure drop offsets the gains in heat transfer in terms

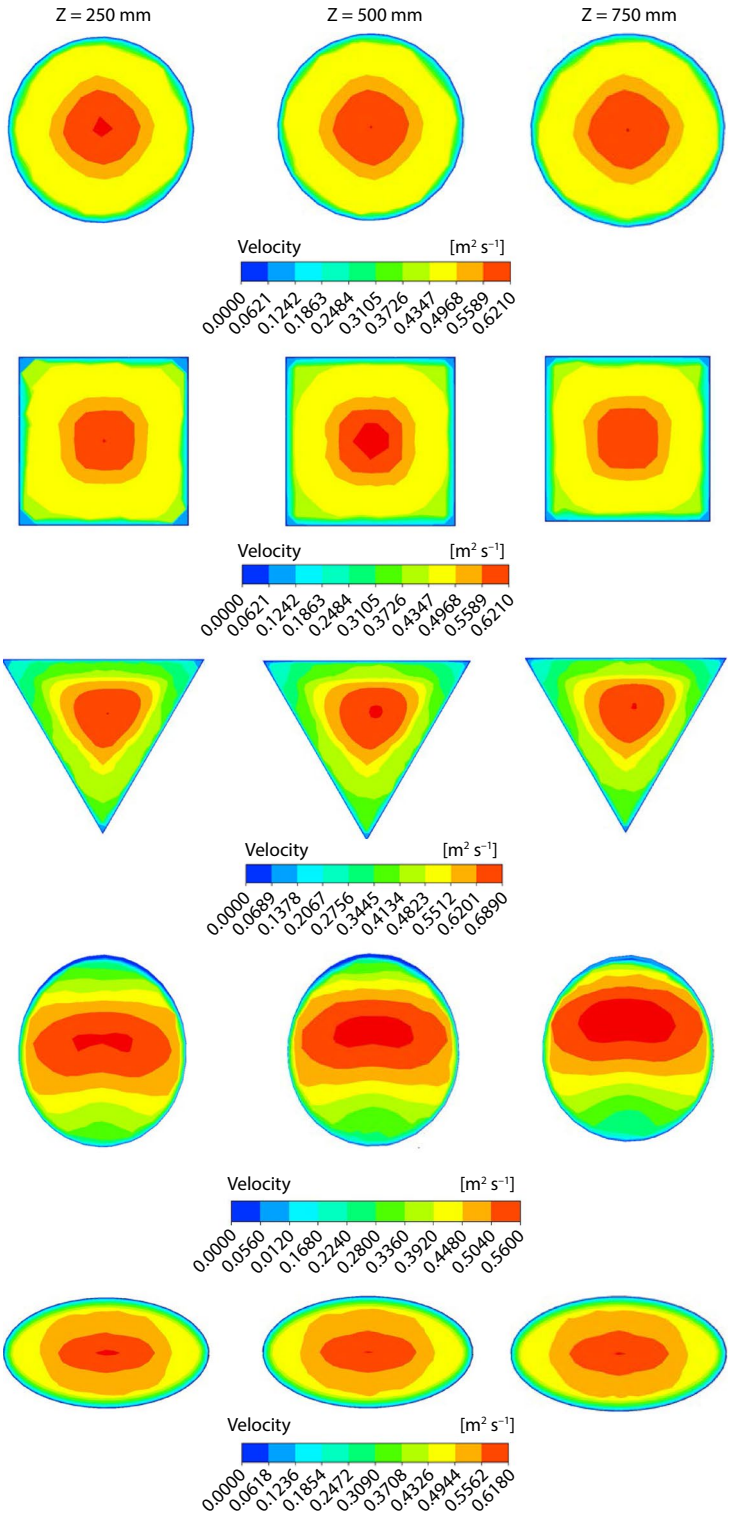

Fig. 13 Contours of velocity magnitude across various cross section planes along the duct length

of pumping power. It is observed that for all the duct geometries, friction factor (f) increases with an increase in Reynolds number (Re). For the serpentine duct, the f is highest for all Re compared to other duct geometries (Fig. 11). This is attributed to lower boundary layer thickness at higher flow rates and subsequently lower viscous resistance. The pressure drop in square duct is the least among them and elliptical, circular and triangular have almost similar characteristics.

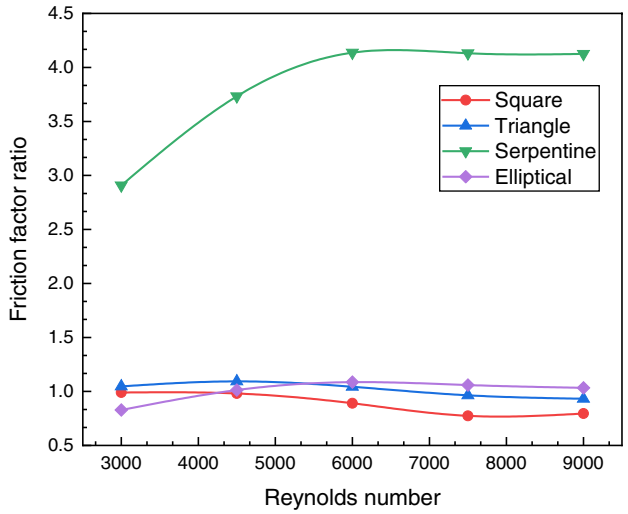

Fig. 14 Variation of Friction factor ratio with Reynolds number for different geometries

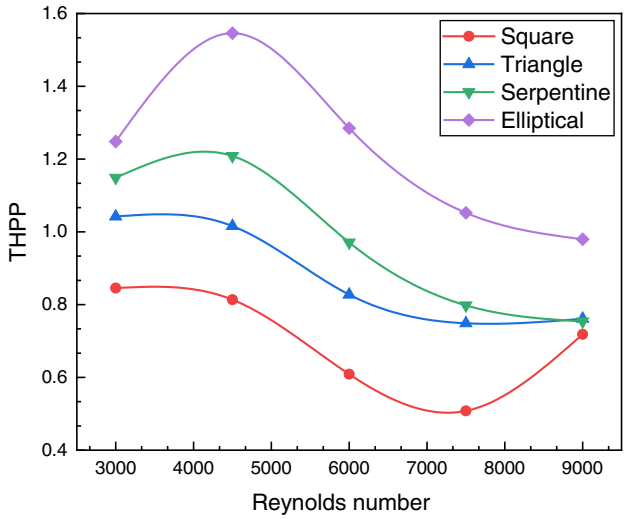

Fig. 15 Variation of Thermo-hydraulic performance parameter with Reynolds number for different geometries

For various cross section planes, as shown in Fig. 12, it is observed that static pressure variation within the plane is higher in serpentine ducts due to the presence of crests and troughs, and the non-uniformity increases along the length. This is attributed to the crests and troughs leading to higher resulting secondary flow velocity (Fig. 8). Whereas in square duct this non-uniformity in pressure distribution is minimal with lower secondary flow velocity. From the velocity magnitude contours (Fig. 13), it is evident that the boundary layer thickness is higher for the serpentine duct and hence higher viscous resistance.

Further, upon comparison, it is noted that the average flow velocity is lower for serpentine ducts resulting in a higher friction factor. The average flow velocity is highest in the square duct leading to the lowest friction factor. Although in a triangular duct, the maximum velocity is higher, the average velocity is lower than that of a square duct due to lower velocity near the corners extending to larger area. Upon comparing the enhancement in f considering circular as the reference geometry, it is evident that serpentine duct and square duct have the highest and lowest values, respectively (Fig. 14).

Thermo-hydraulic performance parameter

As the viscosity of nanofluids is higher, the heat transfer enhancement with the use of nanofluids should be compared to the additional pressure drop within the duct. Hence, the thermo-hydraulic performance parameter (THPP) is evaluated by considering the circular duct as the reference case. It is observed that maximum THPP is attained at Re = 4500 for serpentine and elliptical ducts. With a further increase in

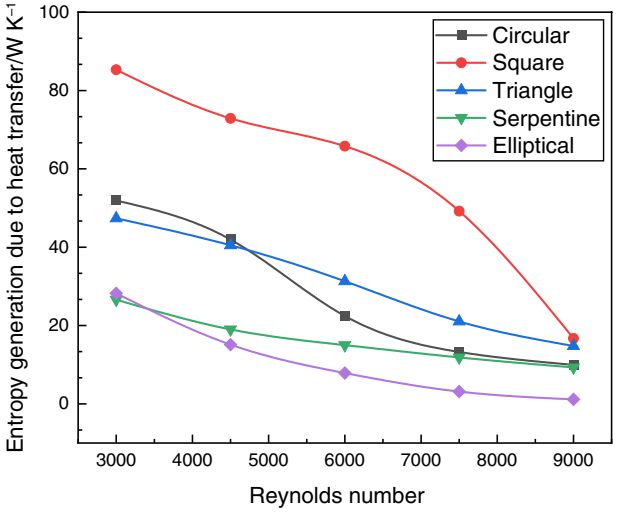

Fig. 16 Variation of entropy generation due to heat transfer with Reynolds for different duct geometries

Re, thermo-hydraulic performance parameter of serpentine and elliptical ducts decreases. For Re ≥ 4500, serpentine duct underperforms the circular duct and for Re > 7500, the elliptical duct shows underperformance. The triangular duct has higher THPP only for lower Re,; whereas, the square duct has THPP < 1 for all Re. Even though the highest enhancement in heat transfer rate is obtained for the serpentine duct, maximum of THPP = 1.54 is obtained for elliptical geometry at Re = 4500. This is attributed to significantly lower pressure drop features than the serpentine duct. The square duct has the lowest THPP owing to lower heat transfer enhancement rate.

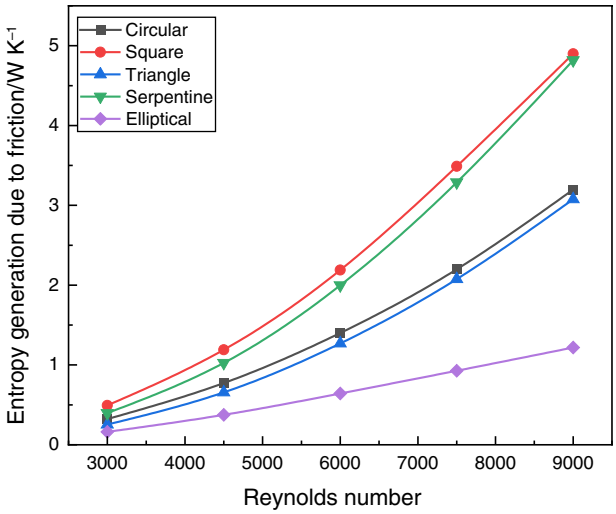

Fig. 17 Variation of entropy generation due to fluid friction with Reynolds number for different geometries

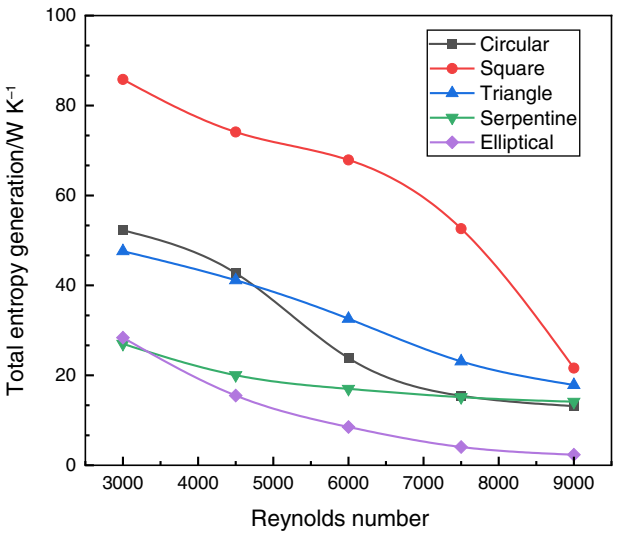

Fig. 18 Variation of total entropy generation with Reynolds number varying from 3000 to 9000 for different geometries

Entropy generation

In this section, entropy generation analysis for different ducts is presented. Entropy generation considers the thermal resistance during heat transfer as well as resistance to the fluid flow. [42] in heat transfer leads to a decrease in entropy and irreversibility in contrast to increasing pressure drop causes increased irreversibility and loss in exergy in systems. Therefore, to select the best-performing geometry it is essential to carry out second law analysis and analyze the quality of heat transfer. Further, the same can be used to find the optimum operating conditions for a particular geometry (Fig. 15).

The entropy generation rate due to heat transfer decreases with an increase in Re, as shown in Fig. 16. As the Re increases, the heat transfer rate increases attributed to lower thermal boundary layer thickness. With better heat transfer, the wall temperature is reduced, resulting in a lower temperature gradient. Hence, at higher Re, the irreversibilities in heat transfer reduce, and subsequently, the entropy generation rate due to heat transfer decreases. For lower Re, square duct has the highest entropy generation and the lowest is obtained for serpentine and elliptical ducts. This is attributed to the presence of secondary flow with larger velocity and the flow separation-re-attachment because of the presence of crest and trough in serpentine duct. For the entire range of Re, elliptical duct has the lowest entropy generation rate due to heat transfer and the highest is exhibited by square duct.

The variation of entropy generation rate due to fluid friction with Re is shown in Fig. 17. For all the duct geometries, entropy generation due to fluid friction increases with an increase in flow velocity due to a higher pressure drop. The square and serpentine ducts have the highest entropy generation; whereas, elliptical duct has the lowest for the range of Re. To account for entropy generation rate due to heat transfer and fluid friction, the variation of total entropy generation with Re is obtained as shown in Fig. 18. It is observed that for the present study, the relative magnitude of entropy generation due to fluid friction is lower than the entropy generation due to heat transfer rate. This is due to the reason that all the duct geometries studied have smooth walls. Total entropy generation rate is highest at lower Re for all the duct geometries studied. Elliptical and serpentine ducts have the lowest entropy generation rate at lower Re and the highest is attributed by the square geometry (Fig. 19). At higher Re, all the geometries have total entropy generation rate in a similar range except elliptical displaying the lowest.

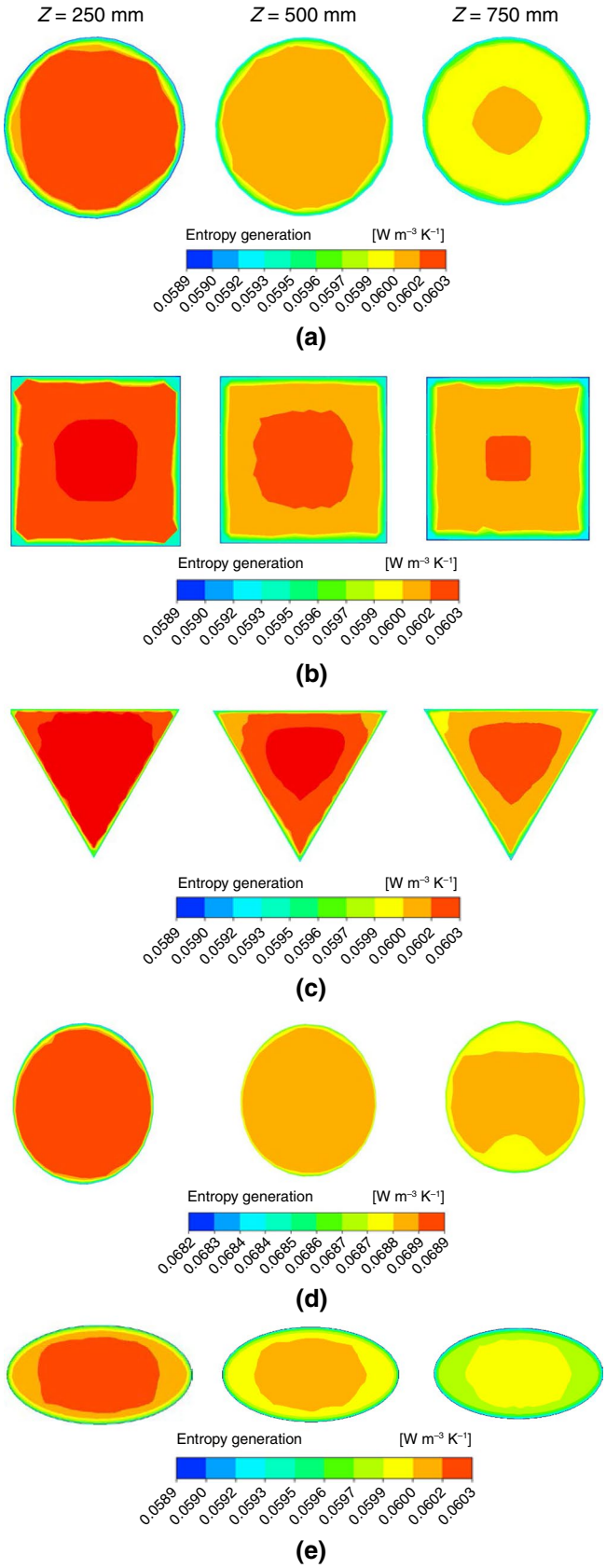

Fig. 19 Total entropy generation contours at $x = 250$, 500, 750 mm cross-planes for **a** circular, **b** square, **c** triangular, **d** serpentine, **e** elliptical geometry for Re = 4500

Conclusions

A 3-D two-phase CFD simulation of nanofluid in various duct configurations has been studied using a mixture model to analyze the impact of duct cross section on the thermo-hydraulic performance in the turbulent flow regime ($3000 < Re < 9000$). The simulations have been carried out for similar hydraulic diameter, length, and heat input. Apart from fluid flow and heat transfer, entropy generation analysis has been carried out to evaluate the quality of heat transfer. The following notable conclusions are drawn based on the analysis:

(a) Maximum enhancement of 86% in *Nu* is obtained for serpentine duct compared to the conventional circular duct at $Re = 4500$. Whereas a square duct underperforms the circular duct with a reduction of 20% in *Nu*. For $Re > 4500$, both square and triangular ducts have lower heat transfer characteristics than the circular duct.
(b) Higher value of TKE was noticed for serpentine and elliptical at the walls of the duct leading to better heat transfer.
(c) An additional increase of 2.73 times in friction factor is obtained for serpentine duct compared to conventional circular duct at $Re = 4500$ owing to the presence of crest and troughs. For all other ducts, the increase in pressure drop is not significant relative to circular duct.
(d) Due to significantly lower increase in pressure drop, elliptical duct has highest thermo-hydraulic performance parameter of 1.54. For $Re > 7500$, elliptical duct showed marginally higher performance. Whereas other ducts configurations underperformed the circular duct for higher Re.
(e) Entropy generation rate decreased with increase in flow velocity and at higher Re, all the duct configurations have similar entropy generation characteristics. At $Re = 4500$, square duct reported highest entropy generation due to heat transfer with an increase of 60% relative to circular duct. Whereas elliptical duct displayed lowest entropy generation, 54% lower than circular duct.
(f) At higher Re, the entropy generation characteristics were not significantly varying as it was for lower Re.

From the above observations, it can be concluded that for the same operating conditions elliptical geometry performed the best with good heat transfer rate and low friction factor and is preferable duct geometry for application involving nanofluid at lower Re. With the above results, elliptical collector can be employed in various thermal applications to enhance the thermo-hydraulic performance at lower Re.

Author contribution AV contributed to conceptualization, data curation, investigation, methodology, and writing—original draft. KN contributed to conceptualization, methodology, writing—original draft, and writing—review & editing, Supervision.

Funding Open access funding provided by Manipal Academy of Higher Education, Manipal.

References

1. Xuan Y, Li Q. Investigation on convective heat transfer and flow features of nanofluids. J Heat Transfer. 2003;125(1):151–5. https://doi.org/10.1115/1.1532008.
2. Masuda H, Ebata A, Teramae K, Hishinuma N. Alteration of thermal conductivity and viscosity of liquid by dispersing ultra-fine particles. Dispersion of Al_2O_3, SiO_2 and TiO_2 ultra-fine particles. Netsu Bussei. 1993;7(4):227–33. https://doi.org/10.2963/jjtp.7.227.
3. Delouei AA, Sajjadi H, Ahmadi G. The effect of piezoelectric transducer location on heat transfer enhancement of an ultrasonic-assisted liquid-cooled CPU radiator. Iranian J Sci Technol Trans Mech Eng. 2023. https://doi.org/10.1007/s40997-023-00667-5.
4. Eastman JA, Choi SUS, Li S, Yu W, Thompson LJ. Anomalously increased effective thermal conductivities of ethylene glycol-based nanofluids containing copper nanoparticles. Appl Phys Lett. 2001;78(6):718–20. https://doi.org/10.1063/1.1341218.
5. Xie H, Wang J, Xi T, Liu Y. Thermal conductivity of suspensions containing nanosized SiC particles. Int J Thermophys. 2002;23(2):571–80. https://doi.org/10.1023/A:1015121805842.
6. Das SK, Putra N, Thiesen P, Roetzel W. Temperature dependence of thermal conductivity enhancement for nanofluids. J Heat Transfer. 2003;125(4):567–74. https://doi.org/10.1115/1.1571080.
7. Wen D, Ding Y. Experimental investigation into convective heat transfer of nanofluids at the entrance region under laminar flow conditions. Int J Heat Mass Transf. 2004;47(24):5181–8. https://doi.org/10.1016/j.ijheatmasstransfer.2004.07.012.
8. Chon CH, Kihm KD, Lee SP, Choi SU. Empirical correlation finding the role of temperature and particle size for nanofluid (Al_2O_3) thermal conductivity enhancement. Appl Phys Lett. 2005. https://doi.org/10.1063/1.2093936.
9. Chopkar M, Das PK, Manna I. Synthesis and characterization of nanofluid for advanced heat transfer applications. Scr Mater. 2006;55(6):549–52. https://doi.org/10.1016/j.scriptamat.2006.05.030.
10. Hwang Y, Park HS, Lee JK, Jung WH. Thermal conductivity and lubrication characteristics of nanofluids. Curr Appl Phys. 2006;6:e67–71. https://doi.org/10.1016/j.cap.2006.01.014.
11. Li CH, Peterson GP. Experimental investigation of temperature and volume fraction variations on the effective thermal

conductivity of nanoparticle suspensions (nanofluids). J Appl Phys. 2006. https://doi.org/10.1063/1.2191571.
12. Yu W, France DM, Routbort JL, Choi SUS. Review and comparison of nanofluid thermal conductivity and heat transfer enhancements. Heat Transfer Eng. 2008;29(5):432–60. https://doi.org/10.1080/01457630701850851.
13. Xie H, Wang J, Xi T, Liu Y, Ai F. Dependence of the thermal conductivity of nanoparticle-fluid mixture on the base fluid. J Mater Sci Lett. 2002;21(19):1469–71. https://doi.org/10.1023/A:1020060324472.
14. Lone SA, Ali F, Saeed A, Bognár G. Irreversibility analysis with hybrid cross nanofluid of stagnation point and radiative flow (TiO_2 + CuO) based on engine oil past a stretchable sheet. Heliyon. 2023;9(4): e15056. https://doi.org/10.1016/j.heliyon.2023.e15056.
15. Saha G, Paul MC. Investigation of the characteristics of nanofluids flow and heat transfer in a pipe using a single phase model. Int Commun Heat Mass Transfer. 2018;93:48–59. https://doi.org/10.1016/j.icheatmasstransfer.2018.03.001.
16. Demir H, Dalkilic AS, Kürekci NA, Duangthongsuk W, Wongwises S. Numerical investigation on the single phase forced convection heat transfer characteristics of TiO_2 nanofluids in a double-tube counter flow heat exchanger. Int Commun Heat Mass Transfer. 2011;38(2):218–28. https://doi.org/10.1016/j.icheatmasstransfer.2010.12.009.
17. Ahmed MA, Yaseen MM, Yusoff MZ. Numerical study of convective heat transfer from tube bank in cross flow using nanofluid. Case Stud Therm Eng. 2017;10:560–9. https://doi.org/10.1016/j.csite.2017.11.002.
18. Xuan Y, Roetzel W. Conceptions for heat transfer correlation of nanofluids. Int J Heat Mass Transf. 2000;43(19):3701–7. https://doi.org/10.1016/S0017-9310(99)00369-5.
19. Khanafer K, Vafai K, Lightstone M. Buoyancy-driven heat transfer enhancement in a two-dimensional enclosure utilizing nanofluids. Int J Heat Mass Transf. 2003;46(19):3639–53. https://doi.org/10.1016/S0017-9310(03)00156-X.
20. Mojarrad MS, Keshavarz A, Shokouhi A. Nanofluids thermal behavior analysis using a new dispersion model along with single-phase. Heat Mass Transf. 2013;49(9):1333–43. https://doi.org/10.1007/s00231-013-1182-3.
21. Kumar S, Prasad SK, Banerjee J. Analysis of flow and thermal field in nanofluid using a single phase thermal dispersion model. Appl Math Model. 2010;34(3):573–92. https://doi.org/10.1016/j.apm.2009.06.026.
22. Özerinç S, Yazıcıoğlu AG, Kakaç S. Numerical analysis of laminar forced convection with temperature-dependent thermal conductivity of nanofluids and thermal dispersion. Int J Therm Sci. 2012;62:138–48. https://doi.org/10.1016/j.ijthermalsci.2011.10.007.
23. Heris SZ, Esfahany MN, Etemad G. Numerical investigation of nanofluid laminar convective heat transfer through a circular tube. Numeri Heat Transf A Appl. 2007;52(11):1043–58. https://doi.org/10.1080/10407780701364411.
24. Maïga SEB, Nguyen CT, Galanis N, Roy G. Heat transfer behaviours of nanofluids in a uniformly heated tube. Superlattices Microstruct. 2004;35(3–6):543–57. https://doi.org/10.1016/j.spmi.2003.09.012.
25. Bahiraei M, Hosseinalipour SM. Thermal dispersion model compared with euler-lagrange approach in simulation of convective heat transfer for nanoparticle suspensions. J Dispers Sci Technol. 2013;34(12):1778–89. https://doi.org/10.1080/01932691.2012.751339.
26. Sabu AS, Ali F, Reddy CS, Areekara S, Mathew A. "Insight on the dynamics of hydromagnetic stagnation-point flow of magnetite-water nanofluid due to a rotating stretchable disk: a two-phase modified Buongiorno modeling and simulation. ZAMM–J Appl Math Mech / Zeitschrift für Angewandte Mathematik und Mechanik. 2023. https://doi.org/10.1002/zamm.202100520.
27. Deepak Selvakumar R, Dhinakaran S. Forced convective heat transfer of nanofluids around a circular bluff body with the effects of slip velocity using a multi-phase mixture model. Int J Heat Mass Transf. 2017;106:816–28.
28. Vanaki ShM, Ganesan P, Mohammed HA. Numerical study of convective heat transfer of nanofluids: a review. Renew Sustain Energy Rev. 2016;54:1212–39. https://doi.org/10.1016/j.rser.2015.10.042.
29. Nuim Labib M, Nine MdJ, Afrianto H, Chung H, Jeong H. Numerical investigation on effect of base fluids and hybrid nanofluid in forced convective heat transfer. Int J Therm Sci. 2013;71:163–71. https://doi.org/10.1016/j.ijthermalsci.2013.04.003.
30. Moghadassi A, Ghomi E, Parvizian F. A numerical study of water based Al2O3 and Al_2O_3–Cu hybrid nanofluid effect on forced convective heat transfer. Int J Therm Sci. 2015;92:50–7. https://doi.org/10.1016/j.ijthermalsci.2015.01.025.
31. Mirmasoumi S, Behzadmehr A. Numerical study of laminar mixed convection of a nanofluid in a horizontal tube using two-phase mixture model. Appl Therm Eng. 2008;28(7):717–27. https://doi.org/10.1016/j.applthermaleng.2007.06.019.
32. Siavashi M, Talesh Bahrami HR, Saffari H. Numerical investigation of flow characteristics, heat transfer and entropy generation of nanofluid flow inside an annular pipe partially or completely filled with porous media using two-phase mixture model. Energy. 2015;93:2451–66. https://doi.org/10.1016/j.energy.2015.10.100.
33. Moraveji MK, Ardehali RM. CFD modeling (comparing single and two-phase approaches) on thermal performance of Al_2O_3/water nanofluid in mini-channel heat sink. Int Commun Heat Mass Transfer. 2013;44:157–64. https://doi.org/10.1016/j.icheatmasstransfer.2013.02.012.
34. Bizhaem HK, Abbassi A. Numerical study on heat transfer and entropy generation of developing laminar nanofluid flow in helical tube using two-phase mixture model. Adv Powder Technol. 2017;28(9):2110–25. https://doi.org/10.1016/j.apt.2017.05.018.
35. Delavari V, Hashemabadi SH. CFD simulation of heat transfer enhancement of Al_2O_3/water and Al_2O_3/ethylene glycol nanofluids in a car radiator. Appl Therm Eng. 2014;73(1):380–90. https://doi.org/10.1016/j.applthermaleng.2014.07.061.
36. Peyghambarzadeh SM, Hashemabadi SH, Hoseini SM, Seifi Jamnani M. Experimental study of heat transfer enhancement using water/ethylene glycol based nanofluids as a new coolant for car radiators. Int Commun Heat Mass Trans. 2011;38(9):1283–90. https://doi.org/10.1016/j.icheatmasstransfer.2011.07.001.
37. Ghasemi SE, Ranjbar AA, Hosseini MJ. Numerical study on effect of CuO-water nanofluid on cooling performance of two different cross-sectional heat sinks. Adv Powder Technol. 2017;28(6):1495–504. https://doi.org/10.1016/j.apt.2017.03.019.
38. Roy G, Nguyen CT, Lajoie P-R. Numerical investigation of laminar flow and heat transfer in a radial flow cooling system with the use of nanofluids. Superlattices Microstruct. 2004;35(3–6):497–511. https://doi.org/10.1016/j.spmi.2003.09.011.
39. Behzadmehr A, Saffar-Avval M, Galanis N. Prediction of turbulent forced convection of a nanofluid in a tube with uniform heat flux using a two phase approach. Int J Heat Fluid Flow. 2007;28(2):211–9. https://doi.org/10.1016/j.ijheatfluidflow.2006.04.006.
40. Lotfi R, Saboohi Y, Rashidi AM. Numerical study of forced convective heat transfer of nanofluids: comparison of different approaches. Int Commun Heat Mass Transfer. 2010;37(1):74–8. https://doi.org/10.1016/j.icheatmasstransfer.2009.07.013.
41. Bianco V, Nardini S, Manca O. Enhancement of heat transfer and entropy generation analysis of nanofluids turbulent convection flow in square section tubes. Nanoscale Res Lett. 2011;6(1):252. https://doi.org/10.1186/1556-276X-6-252.

42. Moghaddami M, Mohammadzade A, Esfehani SAV. Second law analysis of nanofluid flow. Energy Convers Manag. 2011;52(2):1397–405. https://doi.org/10.1016/j.enconman.2010.10.002.
43. Hejazian M, Moraveji MK, Beheshti A. Comparative study of Euler and mixture models for turbulent flow of Al_2O_3 nanofluid inside a horizontal tube. Int Commun Heat Mass Transfer. 2014;52:152–8. https://doi.org/10.1016/j.icheatmasstransfer.2014.01.022.
44. Yang Y-T, Tang H-W, Jian S-J. Numerical simulation and optimization of turbulent nanofluids in a three-dimensional wavy channel. Numeri Heat Transf A Appl. 2016;69(10):1169–85. https://doi.org/10.1080/10407782.2015.1125729.
45. Siavashi M, Jamali M. Heat transfer and entropy generation analysis of turbulent flow of TiO_2-water nanofluid inside annuli with different radius ratios using two-phase mixture model. Appl Therm Eng. 2016;100:1149–60. https://doi.org/10.1016/j.applthermaleng.2016.02.093.
46. Yang Y-T, Tang H-W, Zeng B-Y, Jian M-H. Numerical simulation and optimization of turbulent nanofluids in a three-dimensional arc rib-grooved channel. Numeri Heat Transf A Appl. 2016;70(8):831–46. https://doi.org/10.1080/10407782.2016.1214513.
47. Ahmed HE, Yusoff MZ, Hawlader MNA, Ahmed MI, Salman BH, Kerbeet ASh. Turbulent heat transfer and nanofluid flow in a triangular duct with vortex generators. Int J Heat Mass Transf. 2017;105:495–504. https://doi.org/10.1016/j.ijheatmasstransfer.2016.10.009.
48. Sekrani G, Poncet S, Proulx P. Modeling of convective turbulent heat transfer of water-based <math altimg = "si59.gif" overflow = "scroll"> <mrow> <msub> <mrow> <mtext>Al</mtext> </mrow> <mrow> <mn>2</mn> </mrow> </msub> <msub> <mrow> <mtext>O</mtext> </mrow> <mrow> <mn>3</mn> </mrow> </msub> </mrow> </math> nanofluids in an uniformly heated pipe. Chem Eng Sci. 2018;176:205–19. https://doi.org/10.1016/j.ces.2017.10.044.
49. Najafi Khaboshan H, Nazif HR. Heat transfer enhancement and entropy generation analysis of Al_2O_3-water nanofluid in an alternating oval cross-section tube using two-phase mixture model under turbulent flow. Heat Mass Trans. 2018;54(10):3171–83. https://doi.org/10.1007/s00231-018-2345-z.
50. Salami M, Khoshvaght-Aliabadi M, Feizabadi A. Investigation of corrugated channel performance with different wave shapes. J Therm Anal Calorim. 2019;138(5):3159–74. https://doi.org/10.1007/s10973-019-08361-y.
51. Ajeel RK, Saiful-Islam W, Sopian K, Yusoff MZ. Analysis of thermal-hydraulic performance and flow structures of nanofluids across various corrugated channels: an experimental and numerical study. Therm Sci Eng Prog. 2020;19: 100604. https://doi.org/10.1016/j.tsep.2020.100604.
52. Alawi OA, et al. Effects of binary hybrid nanofluid on heat transfer and fluid flow in a triangular-corrugated channel: an experimental and numerical study. Powder Technol. 2022;395:267–79. https://doi.org/10.1016/j.powtec.2021.09.046.
53. Ekiciler R, Arslan K, Turgut O. Application of nanofluid flow in entropy generation and thermal performance analysis of parabolic trough solar collector: experimental and numerical study. J Therm Anal Calorim. 2023;148(14):7299–318. https://doi.org/10.1007/s10973-023-12187-0.
54. Saddouri I, Rejeb O, Semmar D, Jemni A. A comparative analysis of parabolic trough collector (PTC) using a hybrid nanofluid. J Therm Anal Calorim. 2023;148(18):9701–21. https://doi.org/10.1007/s10973-023-12342-7.
55. Khaledi O, Saedodin S, Rostamian SH. The development of a new thermal modeling and heat transfer mechanisms of a compound parabolic concentrator (CPC) based on nanofluids. J Therm Anal Calorim. 2023;148(16):8557–77. https://doi.org/10.1007/s10973-023-11980-1.
56. Lotfi M, Firoozzadeh M, Ali-Sinaei M. Simultaneous use of TiO_2/oil nanofluid and metallic-insert as enhancement of an evacuated tube solar water heater. J Therm Anal Calorim. 2023;148(18):9633–47. https://doi.org/10.1007/s10973-023-12339-2.
57. Mahian O, et al. Recent advances in modeling and simulation of nanofluid flows-Part I: fundamentals and theory. Phys Rep. 2019;790:1–48. https://doi.org/10.1016/j.physrep.2018.11.004.
58. Manninen M, Taivassalo V, Kallio S. On the mixture model for multiphase flow. Technical Research Center of Finland, Espoo
59. Webb RL, Eckert ERG. Application of rough surfaces to heat exchanger design. Int J Heat Mass Transf. 1972;15(9):1647–58. https://doi.org/10.1016/0017-9310(72)90095-6.
60. Yang L, Huang J, Mao M, Ji W. Numerical assessment of Ag-water nano-fluid flow in two new microchannel heatsinks: thermal performance and thermodynamic considerations. Int Commun Heat Mass Transfer. 2020;110: 104415. https://doi.org/10.1016/j.icheatmasstransfer.2019.104415.